Polish Journal of Chemical Technology, 18, 3, 30—38, 10.1515/pjct-2016-0045

Phenol and methylene blue photodegradation over Ti/SBA-15 materials under uv light

Tomasz Olejnik, Sylwia Pasieczna-Patkowska, Adam Lesiuk, Janusz Ryczkowski

University of Maria Curie-Sklodowska, Faculty of Chemistry, Departament of Chemical Technology, pl. Marii Curie-Skłodowskiej 3, 20-031 Lublin, Poland
**Corresponding author: e-mail: janusz.ryczkowski@umcs.eu*

Ordered SBA-15 mesoporous silica supports have been synthesized and used for incorporation of titanium with different Ti/Si weight ratio via incipient wetness impregnation. Titanium tetraisopropoxide (TTIP) was used as a source of Ti. Obtained catalysts were characterized to investigate the chemical framework and morphology by nitrogen sorption measurements, powder X-ray diffraction (XRD), X-ray fluorescence elemental analysis (XRF), transmission electron microscopy (TEM), UV-Vis diffuse reflectance spectroscopy (UV-Vis DRS) and Fourier transform infrared photoacoustic spectroscopy (FT-IR/PAS). The photocatalytic degradation of phenol and methylene blue water solutions were selected as a probe reactions to the photoactivity test of prepared samples and to verify the potential application of these materials for water purification. Experimental results indicate that the photocatalytic activity of Ti/Si mixed materials depends on the adsorption ability of composites and the photocatalytic activity of the titanium oxide.

Keywords: TiO_2, SBA-15, photocatalysis, phenol, methylene blue, FT-IR/PAS.

INTRODUCTION

Large scale use of agrochemicals releases a huge number of chemicals into the environment. Due to the toxic and persistent nature of some agrochemicals, contamination problems arise in water bodies[1]. Some of them are harmful, cause cancer and endocrinal disruptions. Due to their solubility in water they are often found in contaminated groundwater, surface water and effluents of wastewater treatment plants[2]. Most of the pesticides require more effective treatment methods due to their toxicity, high chemical stability and low biodegradability[3]. Numerous studies have been demonstrated that heterogeneous photocatalysis is an effective process to degrade contaminants, for example phenol and methylene blue.

In recent years there has been an extensive interest in the use of semiconductors as photocatalyst for pollutant degradation[4]. These processes are based on the use of UV light irradiation to stimulate the semiconductor materials. During irradiation of semiconductor photocatalyst with UV light, a UV photon is absorbed by photocatalyst and electron (e^-) hole (h^+) pairs are generated. In the presence of water and oxygen the redox reaction produces hydroxyl radicals that can oxidize pollutants or can be used as an anti-microbial agent[5]. The overall mechanism for the process can be represented using following equations:

$$\text{Photocatalytic nanoparticle} + h\nu \rightarrow e^- + h^+ \quad (1)$$

$$e^- + O_2 \rightarrow O_2^- \quad (2)$$

$$h^+ + H_2O \rightarrow OH^\bullet + H^+ \quad (3)$$

$$OH^\bullet + \text{organic waste} \rightarrow CO_2 + H_2O + \text{others} \quad (4)$$

In heterogeneous photocatalysis two reactions occur consecutively; the first reaction is the reduction of oxygen and the second is the oxidation of organic wastes by the hydroxyl radical. During the excitation of photocatalysts nanoparticles, electrons are accumulated in the conduction band, which causes the generation of a hole. Therefore, it is necessary to consume electrons to increase the efficiency of heterogeneous photocatalysis in the presence of a nano photocatalyst; here, the electrons are consumed by the dissolved oxygen[6].

Among metal oxide semiconductors, such as TiO_2, ZnO, ZnS, SnO_2, titania is believed to be the most promising one, because of its high photocatalytic activity, chemical stability, low cost and without risk for environmental or humans[7]. One difficulty arising in the usage of nano TiO_2 catalysts is the separation of catalysts in the end of the photocatalytic process. The filtration problems have been eliminated to a large extent by the development of supported photocatalysts in which metal oxides are immobilized on different adsorbent materials.

Mesoporous silica materials are widely used as catalysts and host for nanomaterials synthesis because of their highly ordered and uniform mesoporous channels and large surface area. Uniform ordered channels of mesoporous materials can control the particle size of TiO_2 and can efficiently prevent particles from agglomeration [8]. Pure silica itself doesn't have any active sites in the structure acting as a photocatalyst. Consequently, introduction of titania as a principal photocatalyst, into the silica structure is important. The methods of synthesizing titania-silica mixed oxides include grafting method[9], precipitation[10] or impregnation followed by solvent evaporation[11]. One of the most popular ordered mesoporous silica materials is MCM-41. The structure of MCM-41 material is characterized by one-dimensional hexagonal, elliptical or spherical parallel channel systems, whose diameter can be even up to 10 nm. The thickness of pore walls is from 0.8 up to 1.2 nm. It crystallizes in the hexagonal system and the particles have a length of 10–20 μm and a width of 2 μm[12]. Another type of silica materials, which is very interesting as support is the hexagonal SBA-15[13]. SBA-15 is characterized by very high pore volumes, thick pore walls and intrinsically combined micro- and mesopores with a high surface area. The pore diameter is usually around 10 nm. Normal SBA-15 particles are in wheat-like morphology, the size of which ranges from several to tens of micrometers. Compared with the pore

diameter, the length of the channel is extraordinarily high, arising from the enormous particle size.

In the present study we have investigated the synthesis of TiO_2/SBA-15 materials by post-synthesis incipient wetness impregnation. The samples were prepared with different Ti content. The physicochemical properties were analyzed using BET surface area, XRD, XRF, TEM, FT-IR/PAS and UV-Vis (DRS) experiments. Photocatalytic activity of the samples has been tested using methylene blue (MB) and phenol (Ph) degradation as the model pollutants and subsequently comparing TiO_2/SBA-15 with commercially available titanium oxide (P25).

EXPERIMENTAL

Sample preparation

The supported TiO_2/SBA-15 adsorbents with various TiO_2 loading were prepared by incipient wetness impregnation. The SBA-15 materials were synthesized with the block copolymer Pluronic P123 (Sigma-Aldrich) and tetraethyl orthosilicate (TEOS; Acros Organics, 98%) following published procedures[14]. In the preparation, 20 g of P123 was dissolved in 622 ml of water and 98 ml of 35% HCl solution (POCh Basic) and the resulting solution was stirred at 40°C until the solution became clear. Then 4.8 g of TEOS was added and stirred at this temperature for 24 h. This mixture was subsequently raised to 100°C and aged at this temperature for 48 h without stirring. After filtration and washing by ethanol, the solid product was dried at 100°C then calcined at 550°C for 5 h to remove the surfactant template.

The TiO_2/SBA-15 materials were prepared by using titanium tetraisopropoxide (TTIP) (Sigma-Aldrich, 90%) as a precursor and SBA-15 as a support. TTIP was mixed with dry ethanol and then SBA-15 was added in appropriate amount to obtain a different molar ratio of Ti/Si. The mixture was stirred by 24 h at room temperature (RT). After filtration and drying at 110°C for 24 h, obtained powders were calcined at 550°C for 6 h.

Sample characterization

The nitrogen adsorption-desorption isotherms were obtained using an ASAP 2420M (Micromeritics). Samples were degassed at 200°C before the measurement. The X-ray diffraction (XRD) patterns were recorded on Empyrean (PANalytical) diffractometer, using Cu K_α (λ = 1.54060 Å) radiation. The data was collected from 0.1–5° (2θ) with resolution step size of 0.02° (small-angle XRD diffraction patterns, SAXRD) and from 13–107° (2θ) with resolution step size of 0.02° (conventional wide-angle XRD patterns). X-ray fluorescence (XRF) elemental analysis was performed using the Axios mAX (PANalytical) spectrometer. In the spectrometer samples were excited by Rh SDS-max X-ray tube with 4 kW rhodium anode. Transmission electron microscopy (TEM) images were recorded on Titan G2 60-300 kV FEI Company, equipped with field emission gun (FEG). Microscopic studies of the catalyst were carried out at an accelerating voltage of the electron beam equal to 300 kV. Scanning electron microscopy (SEM) images were recorded on Quanta 3D FEG FEI Company. The UV-Vis (DRS) spectra were recorded using an Jasco V-660 spectrofotometer fitted with a PIV-756 diffuse reflectance accessory in the 200–900 nm wavelength range with a scanning rate of 400 nm/min. FT-IR/PAS spectra of studied samples were recorded by means of the Bio-Rad Excalibur 3000 MX spectrometer equipped with photoacoustic detector MTEC300 (in the helium atmosphere in a detector) at RT over the 4000–400 cm^{-1} range at the resolution of 4 cm^{-1} and maximum source aperture. Spectra were normalized by computing the ratio of a sample spectrum to the spectrum of a MTEC carbon black standard. A stainless steel cup (internal diameter 10 mm) was filled with sample (thickness < 6 mm). Before each data collection, the photoacoustic cell was purged with dry helium for 5 min. Interferograms of 1024 scans were averaged for each spectrum.

Photocatalytic reactions

The photodegradation of phenol (Ph) (POCh) and methylene blue (MB) (Chempur, >82%) was performed in order to evaluate the photocatalytic activity of prepared TiO_2/SBA-15 materials. The experiments were performed in a glass reactor. This reactor was submerged in a thermostatic bath to keep the temperature at the desired value within ±0.5°C, and was equipped with a radiation source located in the axial position and a quartz sleeve which houses the lamp. This was a Heraeus TQ 150 medium pressure UV lamp featuring a broad, pronounced line spectrum in the ultraviolet and visible range (200 nm to 600 nm) and a high power density of about 150 W/cm^2. The lamp was also cooled by the air flow. The reactor top had several inlets for stirring, sampling, venting and measuring the temperature.

The glass reactor contained 600 ml of phenol or MB solution with an initial concentration 0.1 g/L and 0.01 g/L, respectively. Commercially pure TiO_2 (P25) (Sigma-Aldrich, ≥ 99.5%) was used as a reference photocatalyst: 0.06 g for phenol and 0.006 g for MB. The amount of Ti-Si catalysts used in each experiments was the same as those of reference sample. The mixture was first stirred for 30 min in dark at room temperature to assure the adsorption equilibrium was reached and then the UV lamp was turn on. 5 ml solution was withdrawn at given time intervals during the illumination and filtered through 0.45 μm syringe filters. The change of phenol concentration was monitored using HPLC (Waters, diode array detector) equipment with a C18 PAH column at λ = 281 nm. The concentration of MB was determined by UV-Vis spectroscopy (Shimadzu, UV-2600). The change of MB concentration was monitored at 665 nm wavelength.

RESULTS AND DISCUSSION

N_2 adsorption-desorption isotherms

Figure 1 shows N_2 adsorption isotherms for calcined samples with different amount of titanium and for pure SBA-15. All materials give typical irreversible type IV adsorption isotherms with H1 hysteresis loop as defined by IUPAC[15]. It can be seen from Figure 1 that the isotherms display an initial steep rise at low partial pressure owning to monolayer nitrogen adsorption followed by a well-defined inflection at higher partial pressure of 0.2 to 0.6 for SBA-15 and to 0.4 for titanium catalysts,

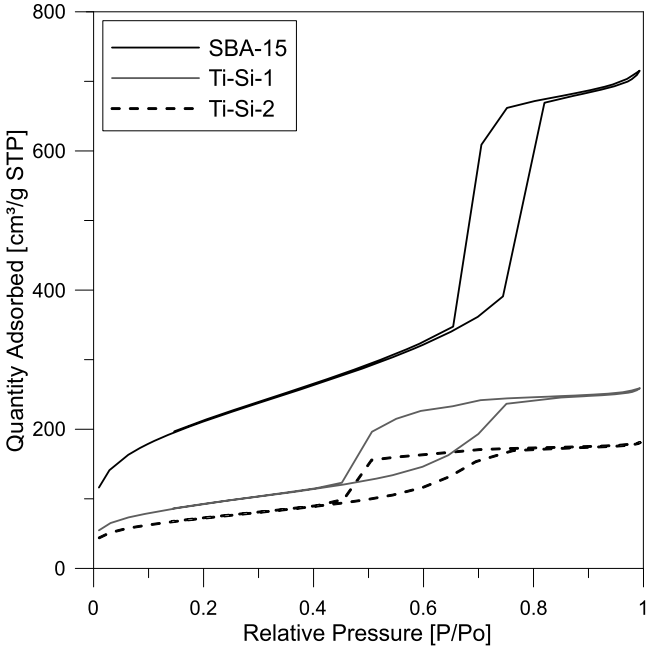

Figure 1. Nitrogen adsorption-desorption isotherms for SBA-15 and Ti-Si structures with different amount of Ti

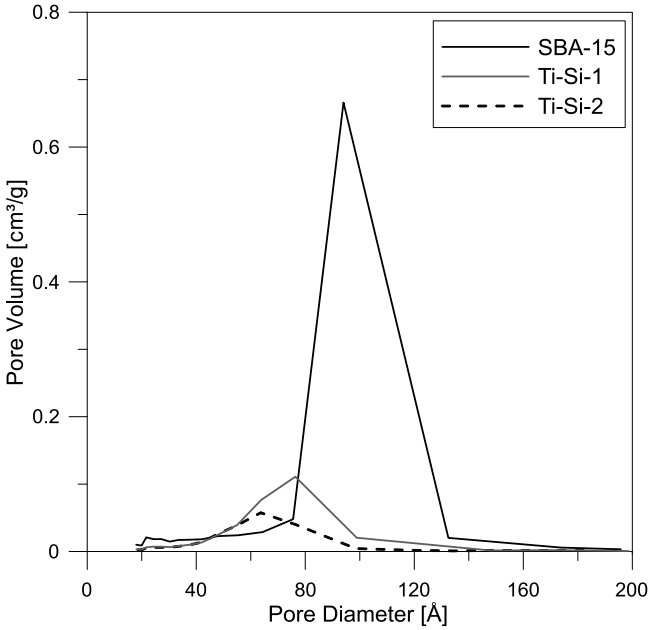

Figure 2. Adsorption average pore width for SBA-15 and Ti-Si structures with different amount of Ti

arising from capillary condensation of nitrogen in the framework-confined mesopores. The hysteresis loops between the adsorption and desorption curves demonstrate that the materials contain large uniform pore size. The structural properties of SBA-15, Ti-Si-1 and Ti-Si-2 are summarized in Table 1. The specific surface area of SBA-15 is 756.9 m^2/g. This value becomes smaller after the impregnation of titanium species on the pores walls of SBA-15. The observation of the decreased surface area may be an indication of the formation of TiO_2 clusters within the mesopores.

pure SBA-15 diffraction patterns, a strong peak at 2θ around 0.9° and two small peaks at 2θ around 1.5° and 1.8°, corresponding to the (100), (110) and (200) reflexes characteristic for the typical hexagonal symmetry p6mm 2D structure. After titanium application on the SBA-15 these peaks are still present and the values of 2θ are slightly shifted, indicating that the layout and structure of the pores are maintained during impregnation. Intensity of the peaks decreases with increasing the Ti/Si ratio. It is understood that the presence of titanium oxide may cause accidental collapse of the mesoporous channels[16].

Table 1. Physicochemical properties of Ti-Si catalysts and pure SBA-15

Sample	BET surface area [m²/g]	Adsorption average pore width [Å]	Total pore volume [cm³/g]	Crystallite size [nm]	Content of titania [%]
SBA-15	756.9	98	1.1	–	–
Ti-Si-1	327.6	75	0.4	24	25
Ti-Si-2	255.1	61	0.2	29	35

The pore size distribution curves obtained from the desorption branch of the nitrogen isotherm by the BJH method are shown in Figure 2. It can be seen that the host SBA-15 has an average pore size of 100 Å, and after the inclusion of TiO_2 nanoparticles, the average pore size decreases up to 75 Å for Ti-Si-1 and to 60 Å for Ti-Si-2. The pore volume of pure SBA-15 is much larger than the samples with incorporated TiO_2, and the average volume is reduced from 0.7 cm^3/g to 0.1 cm^3/g for the Ti-Si-1 or 0.05 cm^3/g for Ti-Si-2. These results confirm the presence of TiO_2 on the mesoporous silica surface.

The titanium content for prepared samples was determined from XRF measurements. It can be noted that by loading 25% and 35% of TiO_2 onto the SBA-15 support the BET surface area of Ti-Si-1 and Ti-Si-2 decreased about 2 and 3 times, respectively. It suggests that TiO_2 was not well dispersed on SBA-15 upon loading.

X-ray diffraction characterization

Small-angle X-ray diffraction patterns are shown in Figure 3. Three diffraction peaks can be observed on

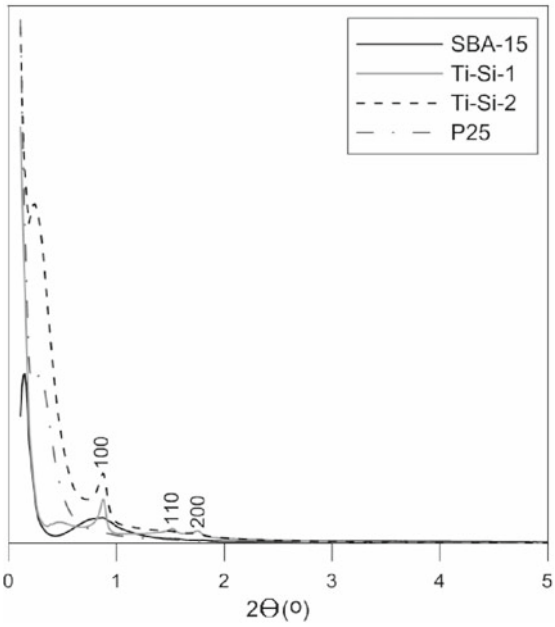

Figure 3. Small angle (SAXRD) patterns of the SBA-15 and Ti-Si with different amount of titanium

Figure 4 shows the wide-angle diffraction patterns. Both mesoporous matrices reveal diffraction patterns with a narrow peak at around $2\theta = 24^{o}$ corresponding to amorphous silica[17]. In all samples the main crystalline form of titanium oxide is anatase, which is indicated by peaks at 25.3°, 37.8°, 48.1°, 55.1° in 2θ angle values corresponding to the reflexes (101), (004) (200) (211) [18].

Crystallite diameters obtained using diffraction studies are usually different from the particle size determined by other techniques such as scanning or transmission electron microscopy. This is due to the fact that in the case of microscopic techniques the grain can be seen, which may consist of number of connected crystallites. The average crystallite size of titanium oxide (Table 1) was determined from the Scherrer equation, based on the width of anatase reflex (101) with the assumption that the crystals have a spherical shape.

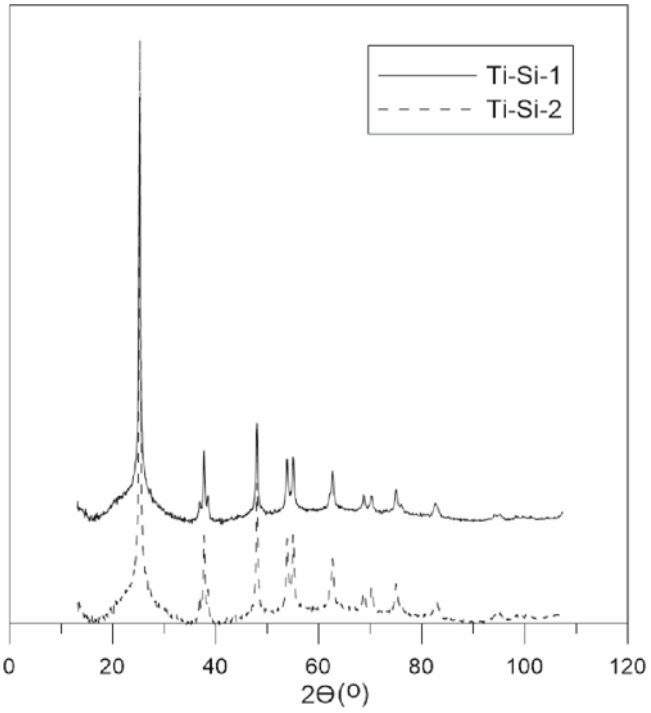

Figure 4. Wide-angle XRD patterns of the SBA-15 and Ti-Si with different amount of titanium

Transmission and scanning electron microscopy characterization

The highly ordered mesostructures of synthesized materials after calcination can be further confirmed by TEM analysis. Figure 5 shows that the highly ordered pore structure of pure SBA-15 described in literature[19, 20] with a pore diameter of about 10 nm is well recognized in image (A). Moreover, the regular silica morphology is at least partially maintained after the TiO_2 impregnation. TEM pictures of Ti-Si-1 and Ti-Si-2 display some small dark spots on the silica walls (Figs. 5B and 5D) which are probably associated with the presence of TiO_2 inside the pores. In Figure 5C TiO_2 can be observed on the external silica surface, which is further supported by the effect of TiO_2 content on pores volume and pores diameter (Table 1). All the images of SBA-15, Ti-Si-1 and Ti-Si-2 show highly ordered hexagonal arrays of the mesoporous materials with uniform pore size, what corresponds with the results obtained using SAXRD. The uniform pore size is in good agreement with the value measured from

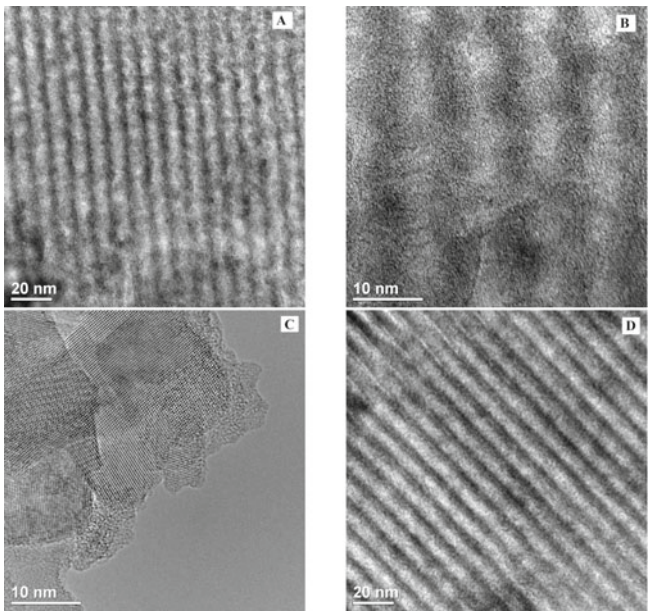

Figure 5. TEM images of prepared materials: (A) SBA-15, (B) and (C) Ti-Si-2, (D) Ti-Si-1

N_2 adsorption-desorption experiments. These pores allow rapid diffusion of various liquid reactants and products during photocatalytic reaction and enhance the rate of photocatalytic reaction. It may be noted that long range mesoporous-ordering characteristic is not disturbed by the addition of TiO_2[21].

The SEM micrographs of synthesized SBA-15 and Ti-Si catalysts are shown in Figure 6. The SEM image of pure SBA-15 presented in Figure 6A shows curved rod-like particles of relatively uniform size with a quite smooth surface[22]. In the Ti-Si-1 and Ti-Si-2 samples, as evidenced from Figure 6B and 6C, these powders show a homogenous distribution of the titanium on the internal surface of SBA-15 powder and the morphology of samples does not change, compared to pure SBA-15.

UV-Vis (DRS) measurements

Figure 7 shows the UV-Vis absorption spectra of prepared catalysts. The initial SBA-15 exhibited no significant absorption in the examined UV-Vis range. The absorption in both visible and UV range increased for the samples with Ti incorporation compared with undoped SBA-15. The absorption changes in the range of 200–450 nm are assigned to the charge transfer (CT) from O 2p orbital (VB) to Ti 3d orbital (CB). It can also be noticed that there is no blue shift in the absorption band edge with the decreasing TiO_2 content[23]. This is consistent with the results of average crystal size (Table 1) and TEM images (Fig. 5.C). It indicates that the distribution of the TiO_2 crystallites on the silica surface is not uniform. In addition, the broaden adsorption peak at about 230 nm is caused by the electron migration between the tetrahedral site of Ti^{4+} and O. This is because the hydrophilic nature of the silica surface, which favors the presence of hydrated titanium in tetrahedral coordination (230 nm) what already has been observed for amorphous silica-supported titanium catalysts[24]. However, the band at about 300 nm may be attributed to titanium in an impaired five fold and six fold coordination in the structure of mesoporous silica[25].

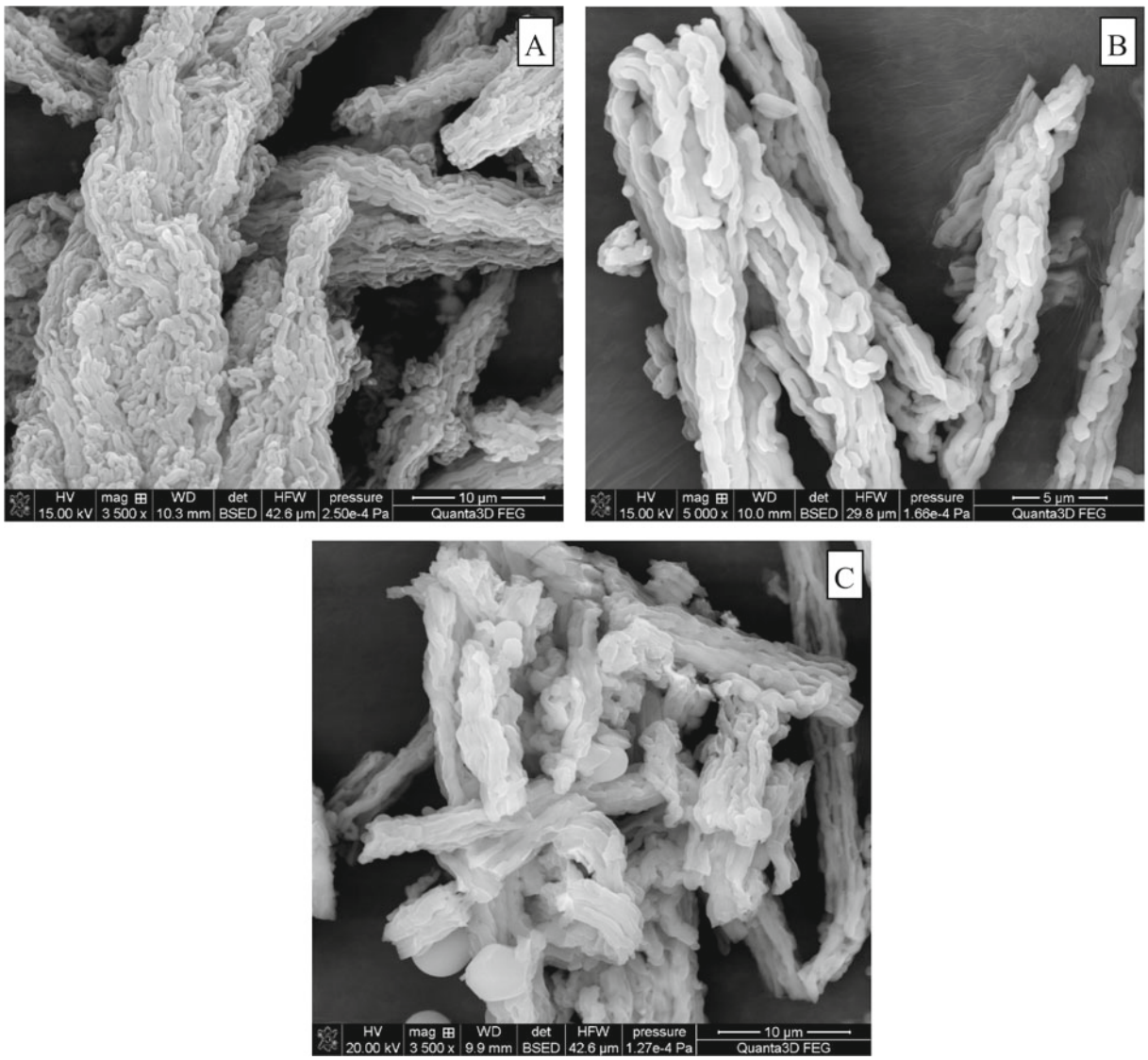

Figure 6. SEM images of prepared materials: (A) SBA-15, (B) Ti-Si-1, (C) Ti-Si-2

The band gap of the commercial TiO_2 samples is 3.2 eV which corresponds to anatase band gap[26]. To calculate the indirect band gap for systems containing anatase, the Tauc method has been used. Band gap energy can be estimated from a plot of $(\alpha h\nu)^{1/2}$ versus photon energy $h\nu$ (Fig. 7), where α is the absorption coefficient and $h\nu$ is a photon energy. The intercept of the tangent to the plot direct gives a good approximation of the band gap energy for indirect band gap materials such TiO_2. The band gap of prepared catalysts are estimated to be ca. 3.2 eV[27].

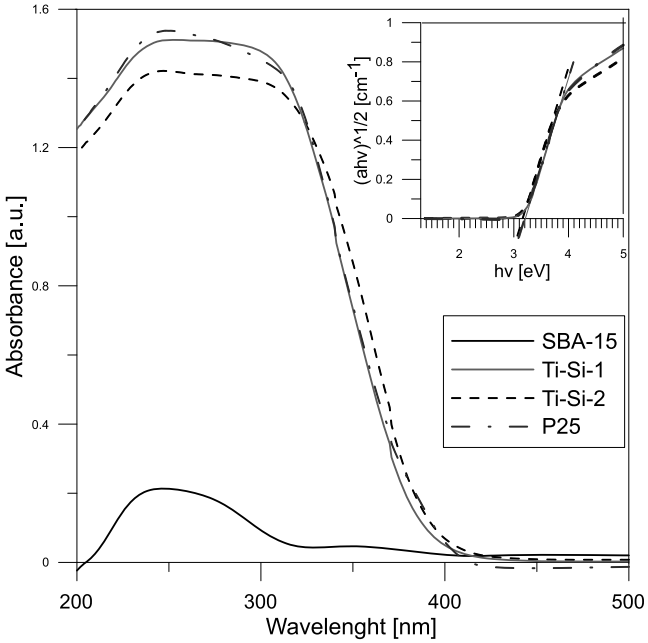

Figure 7. Diffuse reflectance UV-vis absorption spectra of SBA-15, Ti-Si-1 and Ti-Si-2 catalysts and band-gap change for Ti-Si-1, Ti-Si-2 and P25 samples

FT-IR/PAS spectroscopy

The main sample handling problem in the FT-IR analysis of solid materials is that nearly all materials are too opaque in their normal forms for direct transmission analysis in the mid-IR spectral region. One of the major disadvantage of transmission method is the necessity of preparing the pellet from a mixture of tested material and the compound transparent to IR radiation (usually potassium bromide), serving also as a matrix. Application of KBr pelleting may cause deformation and, in consequence, wrong interpretation of the spectrum. Another disadvantage in the use of the transmission method is the hygroscopicity of potassium bromide. The adsorbed water is visible in the IR spectrum at ~3500 and ~1630 cm^{-1} and these bands are intense enough, they can cover bands derived from the sample. The most broadly applicable mid-IR solution to the opacity and

water influence is photoacoustic spectroscopy (FT-IR/PAS)[28]. This technique is non-destructive, can be used in the analysis of materials which are difficult to homogenize, or the structure or the chemical composition change during grinding. FT-IR/PAS allows to obtain a spectrum of the sample without previous preparation.

FT-IR/PAS spectra of the samples are shown in Figure 8 and 9. For the purpose of better visibility, FT-IR/PAS spectra presented further in this work were divided into two ranges: 4000–2200 cm^{-1} (where mainly –OH and C–H groups vibrations are visible) and 2000–400 cm^{-1}. Within the first range (Fig. 8) the sharp band is visible at 3744 cm^{-1} in the spectra of pure SBA-15 and Si-Ti samples. This is a result of overlapping of absorption of truly isolated silanol and of slightly perturbed vicinals of silanols[29]. The band of isolated hydroxyls in the TiO_2 spectrum is visible at 3686 cm^{-1}. Their presence have been recognized to play an important role in the photodegradation process through their interactions with photogenerated holes[30]. The bands within 3700–3000 cm^{-1} are assigned to the H-bonded –OH with various OH…H distances[29]. In all spectra, the bands at about 3435 and 1630 cm^{-1} can be attributed to the stretching vibration of hydroxyl and water, respectively[31]. The bands of aliphatic C-H vibrations (2970–2860 cm^{-1}) are visible in all presented spectra. Their presence indicates incomplete removal of the precursor or surfactant of both TiO_2 and silica. This is a kind of disadvantage, since the residual surfactant can absorb a certain amount of light and thus become a competition for light absorption with the photocatalyst.

The broad, intense double bands appeared in the 1290–1000 cm^{-1} and can be attributed to asymmetric stretching vibrations of Si-O-Si bridges. The peak at 1085 cm^{-1} corresponds to the asymmetric stretching vibration of

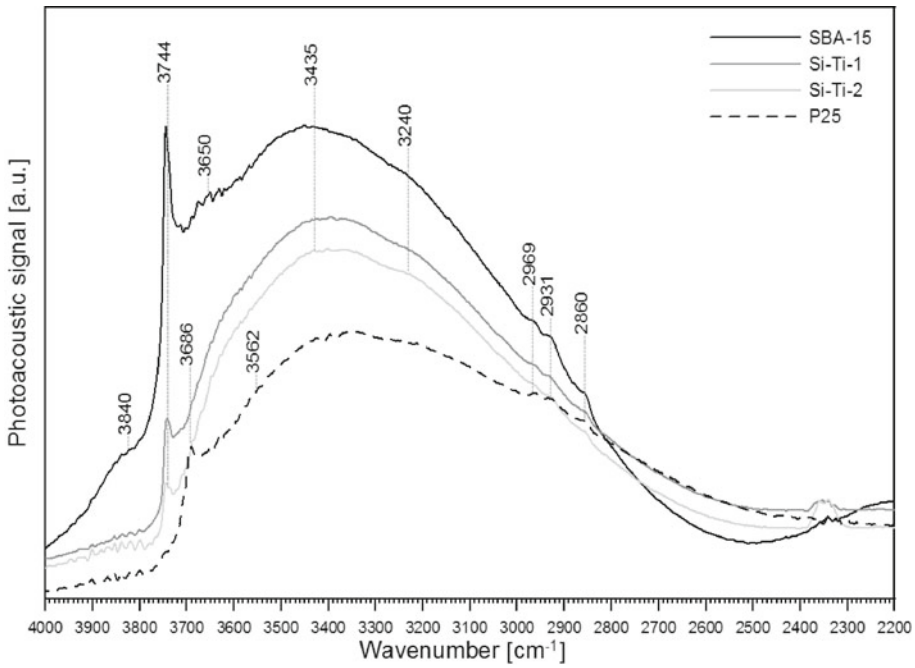

Figure 8. Infrared spectra for SBA-15, Ti-Si-1 and Ti-Si-2 catalysts in the 4000–2200 cm^{-1} range

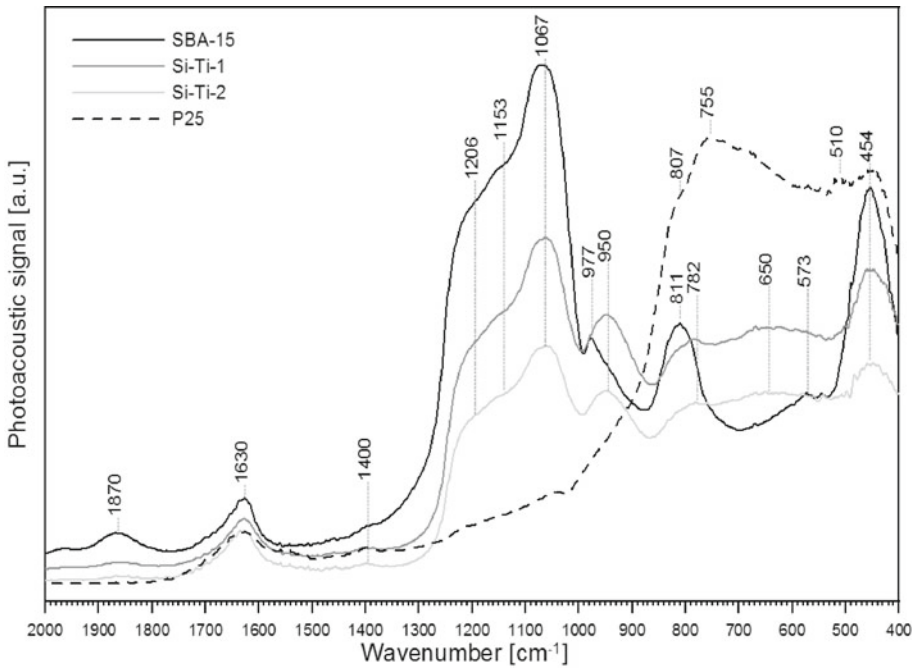

Figure 9. Infrared spectra for SBA-15, Ti-Si-1 and Ti-Si-2 catalysts in the 2000–400 cm^{-1} range

bulk Si–O–Si, and the peaks at 811 and 454 cm^{-1} can be assigned to the symmetric stretching and deformation modes of Si–O–Si, respectively. Theoretically, the IR bands observed within 980–910 cm^{-1} can be assigned to the Si–O–Ti and Si–O–Si stretching vibration[21]. Upon addition of TiO_2 (Ti-Si samples), a shift of about 27 cm^{-1} to lower frequencies can be detected. The band at 950 cm^{-1} is attributed to Si-O-Ti asymmetric stretching vibrations[32]. The shift towards lower wavenumbers is visible also for 811 cm^{-1} band. It may be the proof for incorporation of Ti in silica framework.

Photocatalytic tests

The photocatalytic activity of the Ti-Si catalysts was evaluated in the degradation of phenol and methylene blue model solutions. The objectives catalytic properties was compared with commercial anatase TiO_2 (P25), which is the standard system employed in the field of photocatalytic reactions. In photodegradation experiments there are two factors resulting in the decrease of pollutants: the adsorption on the photocatalysts surface and photodegradation. Figure 10 and 11 shows the degradation curves of phenol and MB for Ti-Si samples with different Ti content and P25. Blank experiments, without addition of the catalyst were also carried out and no photodegradation was observed.

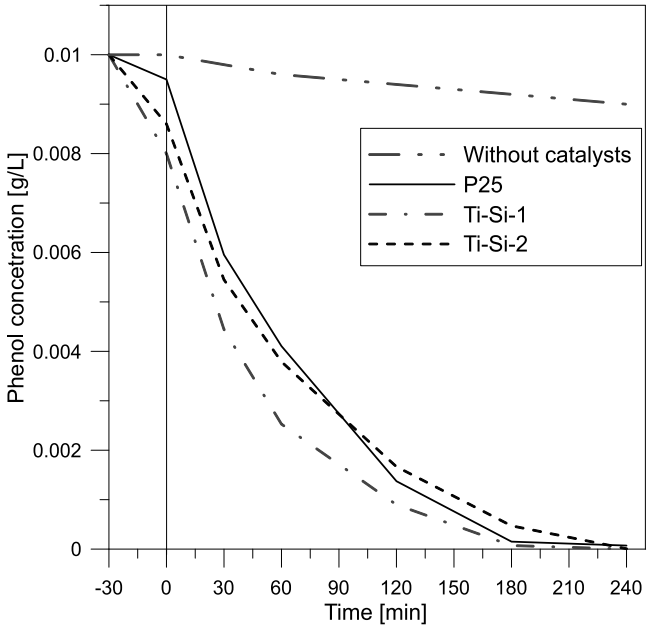

Figure 10. Photocatalytic degradation of phenol on Ti-Si catalysts and pure TiO_2 P25

Adsorption-kinetic models and specifically the Langmuir-Hinshelwood (L-H) model are the most commonly applied to describe photocatalytic mineralization reactions[33]. The L-H based kinetic models relate the rate of surface-catalyzed reactions to the surface covered by the substrate. According to the L-H model, the rate of a unimolecular surface reaction is proportional to the surface coverage. However, as the concentration of the reactants increases above a certain level, the catalyst surface becomes saturated and this may even lead to a decrease in the observed rates. The generation of difficult to degrade intermediates and their continued presence on the surface can also have a negative effect on the degradation rate of their parent compounds[34]. In order

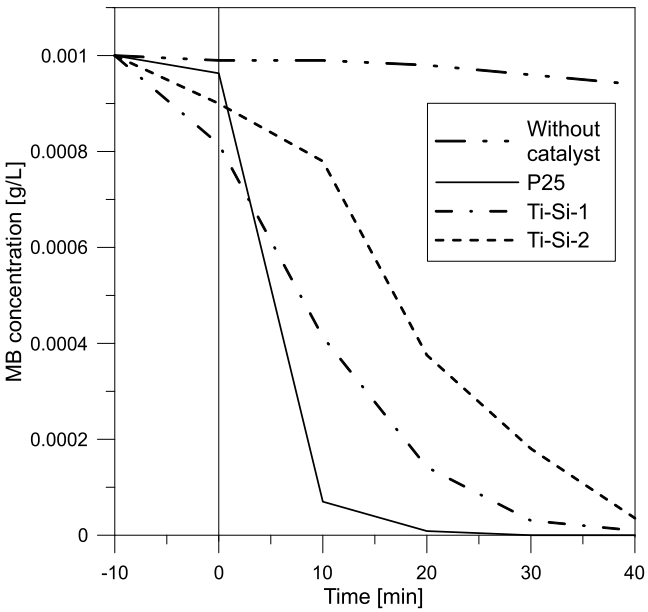

Figure 11. Photocatalytic degradation of methylene blue on Ti-Si catalysts and pure TiO_2 P25

to get the accurate kinetic data, kinetic experiment was carried out after 30 min in dark to assure the adsorption equilibrium was reached. The photocatalytic oxidation of organic pollutants can be represented, according to L-H method, as follows:

$$kt = -\frac{dC}{dt} \tag{5}$$

In addition, it can be integrated as follows:

$$kt = -\ln\left(\frac{C}{C_0}\right) \tag{6}$$

where C_o is the initial concentration of pollutant solution and k is the rate constant.

The apparent rate constant of prepared photocatalysts were calculated and listed in Table 2. In the case of phenol removal, Ti-Si-1 catalyst and P25 have the same, and simultaneously, the highest rate constant (0.026 min^{-1}). But in the case of MB the rate constant decreases in the following order: P25 > Ti-Si-1 > Ti-Si-2. It is generally accepted that for effective degradation, the organic compounds should be concentrated at the TiO_2 surface firstly, and the large surface area of Ti-Si samples also can adsorb significant amounts of water and hydroxyl groups, which react with photoexcited holes on the catalyst surface and can produce hydroxyl radicals[35]. According to Zhang et. al[36], the photocatalytic activity depends on the titania mean particle size, since the nanocrystalline TiO_2 will influence the dynamic of e^-/h^+ recombination. This is probably the cause that Ti-Si-2 catalyst has the worst photocatalytic activity in the removal of both MB and phenol from the model solution.

Table 2. Rate constant of Ti-Si samples and P25 for phenol and MB photodegradation

Catalyst	Rate constant for phenol [min^{-1}]	Rate constant for MB* [min^{-1}]
P25	0.026	0.230
Ti-Si-1	0.026	0.114
Ti-Si-2	0.016	0.079

* methylene blue.

Identification of phenol photodegradation by-products, in the presence of pure TiO_2 and Ti-Si catalysts, was performed by HPLC, using retention time to analyze them qualitatively. However, this method requires the use not only many calibration standards, but also a lot of time because there are many unknown compounds in the intermediates, and some compounds have the same retention time. In photocatalytic experiments the following by-products have been detected: hydroquinone, resorcinol, catechol, 1.2.3-benzenetriol, (E)-2-butenedioic acid, 2-hydroxy-propaldehyde, glycerol, 3-hydroxypropyl acid, and hydroxy-acetic acid. In our case only four of them have been detected: hydroquinone, resorcinol, 1.4-benzoquinone and catechol. It has been reported that $OH^{\bullet}$ radicals attack the phenyl ring, yielding catechol, resorcinol and hydroquinone, then the phenyl rings in these compounds break up to give malonic acid, then short-chain organic acids such as maleic, oxalic, acetic, formic, and finally CO_2. The production of $OH^{\bullet}$ radicals takes place as follows: TiO_2 under the ultraviolet radiation gives rise to electron-hole pairs on the surface, which react with water molecules to give $OH^{\bullet}$. During the process H^+ or $H^{\bullet}$ is scavenged by oxygen to form $HO_2^{\bullet}$ radicals, which finally convert to $OH^{\bullet}$ radicals. Therefore, the principal reaction leading to organics decomposition would be the one with $OH^{\bullet}$ radicals. Based on the intermediates detected in this experiment, it can be concluded that $H^{\bullet}$ also takes part in the photodegradation. $H^{\bullet}$ may be produced through three routes: (1) water molecules react with holes in the electron-hole pairs to produce $OH^{\bullet}$ and H^+, H^+ combines with the electron from the electron-hole pairs; (2) during the process of $OH^{\bullet}$ attacking the aromatic ring, carbon – hydrogen bond breaks up, hydrogen is substituted for $OH^{\bullet}$, and $H^{\bullet}$ is produced; (3) whether TiO_2 exists or not, the main intermediates detected are the same and UV only provides energy to break covalent bonds, $H^{\bullet}$ may also be produced by the break of oxygen – hydrogen bond in water molecules and phenol molecules; or carbon – hydrogen in phenol molecules. For UV, the energy of wavelength 253.7 nm is equal to 472 kJ/mol, which is higher than the H-O bond energy (462.8 kJ/mol), C-H (413.0 kJ/mol), C-O (357.7 kJ/mol), so these bonds probably break upon UV irradiation[37].

CONCLUSIONS

Titania-containing ordered mesoporous silica (SBA-15) has been synthesized with different Ti/Si weight ratios using sol-gel impregnation method and characterized by several physical techniques. Ordered mesoporous SBA-15 type with textural porosity has a major effect on the structural properties and photocatalytic activity. The results demonstrate that the order of the SBA-15 framework was maintained upon impregnation by titanium tetraisopropoxide. The increase of titanium amount led to decrease of the surface area and random dispersion of titanium nanoparticles inside the channels of SBA-15 thus narrowing parts of the SBA-15 mesopores. The results of photodegradation activity indicate the influence of TiO_2 content on the photocatalytic activity of the TiO_2/SBA-15 materials. It can be seen that the Ti-Si-1 and Ti-Si-2 catalysts completely degrade phenol and methylene blue under UV light irradiation after 180 min and 40 min, respectively. Thus Ti-Si mesoporous materials exhibit potential application in the photodegradation of toxic pollutants in environment.

ACKNOWLEDGEMENT

The research was carried out with the equipment purchased thanks to the financial support of the European Regional Development Fund in the framework of the Polish Innovation Economy Operational Programme (contract no. POIG.02.01.00-06-024/09 Centre for Functional Nanomaterials).

LITERATURE CITED

1. Oller, I., Gernjak, W., Maldonado, M.I., Perez-Estrada, L.A., Sanchez-Perez, J.A. & Malato, S. (2006). Solar photocatalytic degradation of some hazardous water-soluble pesticides at pilot-plant scale. *J. Hazard. Mater*. 138, 507–517. DOI: 10.1016/j.jhazmat.2006.05.075.

2. Parra, S., Sarria, V., Malato, S., Peringer, P. & Pulgarin, C. (2000). Photochemical versus coupled photochemical-biological flow system for the treatment of two biorecalcitrant herbicides: metobromuron and isoproturon. *Appl. Catal. B: Environ*. 27, 153–168. DOI: 10.1016/S0926-3373(00)00151-X.

3. Gogate, P.R. & Pandit, A.B. (2004). A review of imperative technologies for wastewater treatment I: oxidations technologies at ambient conditions. *Adv. Environ. Res*. 8, 501–551. DOI: 10.1016/S1093-0191(03)00032-7.

4. Kitano, M., Matsuoka, M., Ueshima, M. & Anpo, M. (2007). Recent developments in titanium oxide-based photocatalysts. *Appl. Catal. A: Gen*. 325, 1–14. DOI: 10.1016/j.apcata.2007.03.013.

5. Rawat, J., Rana, S., Srivastava, R. & Misra, R.D.K. (2007). Antimicrobial activity of composite nanoparticles consisting of titania photocatalytic shell and nickel ferrite magnetic core. *Mater. Sci. Eng*. C 27, 540–545. DOI: 10.1016/j.msec.2006.05.021.

6. Sarkar, S., Das, R., Choi, H. & Bhattacharjee, C. (2014). Involvement of process parameters and various modes of application of TiO_2 nanoparticles in heterogeneous photocatalysis of pharmaceutical wastes – a short review. *RSC. Adv*. 4, 57250–57266. DOI: 10.1039/C4RA09582K.

7. Legrini, O., Oliveros, E. & Braun, A.M. (1993). Photochemical processes for water treatment. *Chem. Rev*. 93(2), 671–698. DOI: 10.1021/cr00018a003.

8. Yang, H., Deng, Y. & Du, C. (2009). Synthesis and optical properties of mesoporous MCM-41 containing doped TiO_2 nanoparticles. *Colloids Surf. A: Physicochem. Eng. Aspects* 339, 111–-117. DOI: 10.1016/j.colsurfa.2009.02.005.

9. Yan, W., Chen, B., Mahurin, S.M., Hagaman, E.W., Dai, S. & Overbury, S.H. (2004). Surface sol-gel modification of mesoporous silica materials with TiO_2 for the assembly of ultrasmall gold nanoparticles. *J. Phys. Chem. B* 108(9), 2793–2796. DOI: 10.1021/jp037713z.

10. Hanprasopwattana, A., Srinivasan, S., Sault, A.G. & Datye, A.K. (1996). Titania coatings on monodisperse silica spheres (characterization using 2-propanol dehydratation and TEM). *Langmuir* 12(13), 3173–3179. DOI: 10.1021/la950808a.

11. Hsien, Y.H., Chang, C.F., Chen, Y.H. & Cheng, S. (2001). Photodegradation of aromatic pollutants in water over TiO_2 supported on molecular sieves. *Appl. Catal. B: Environ*. 31, 241–249. DOI: 10.1016/S0926-3373(00)00283-6.

12. Bhaumik, A. & Tatsumi, T. (2000). Organically Modified Titanium-Rich Ti-MCM-41, Efficient Catalysts for Epoxidation Reactions. *J. Catal*. 189, 31–39. DOI: 10.1006/jcat.1999.2690.

13. Segura, Y., Cool, P., Van Der Voort, P., Mees, F., Meynen, V. & Vansant, E.F. (2004). TiO_x-VO_x mixed oxides on SBA-15 support prepared by the designed dispersion of acetylacetonate

complexes: spectroscopic study of the reaction mechanisms. *J. Phys. Chem. B* 108, 3794–3800. DOI: 10.1021/jp036259w.
14. Zhao, D.Y., Huo, Q., Feng, J., Chmelka, B.F. & Stucky, G.D. (1998). Nonionic triblock and star diblock copolymer and oligomeric surfactant syntheses of highly ordered, hydrothermally stable, mesoporous silica structures. *J. Am. Chem. Soc*. 120(24), 6024–6036. DOI: 10.1021/ja974025i.
15. Sing, K.S.W., Everett, D.H., Haul, R.A.W., Moscow, L., Pierotti, R.A., Rouqerol, J. & Siemieniewska, T. (1985). Reporting physisorption data for gas/solid systems with special reference to the determination of surface area and porosity. *Pure Appl. Chem*. 57, 603–619. DOI: 10.1351/pac198557040603.
16. Busuioc, A.M., Meynen, V., Beyers, E., Mertens, M., Cool, P., Bilba, N. & Vansant, E.F. (2006). Structural features and photocatalytic behaviour of titania deposited within the pores of SBA-15. *Appl. Catal. A: Gen*. 312, 153–164. DOI: 10.1016/j.apcata.2006.06.043.
17. Tuel, A. & Hubert-Pfalzgraf, L.G. (2003). Nanometric monodispersed titanium oxide particles on mesoporous silica: synthesis, characterization, and catalytic activity in oxidation reactions in the liquid phase. *J. Catal*. 217, 343–353. DOI: 10.1016/S0021-9517(03)00078-2.
18. Newalkar, B.L., Olanrewaju, J. & Komarneni, S. (2001). Direct synthesis of titanium substituted mesoporous SBA-15 molecular sieve under microwave-hydrothermal conditions. *Chem. Mater*. 13(2), 552–557. DOI: 10.1021/cm000748g.
19. Zhao, D., Feng, J., Huo, Q., Melosh, N., Fredrickson, G.H., Chmelka, B.F. & Stucky, G.D. (1998). Triblock Copolymer Syntheses of Mesoporous Silica with Periodic 50 to 300 Angstrom Pores. *Science* 279, 548–552. DOI: 10.1126/science.279.5350.548.
20. Ding, H., Sun, H. & Shan, Y. (2005). Preparation and characterization of mesoporous SBA-15 supported dye-sensitized TiO_2 photocatalyst. *J. Photochem. Photobiol. A: Chem*. 169, 101–107. DOI: 10.1016/j.jphotochem.2004.04.015.
21. Qiao, W.T., Zhou, G.W., Zhang, X.T. & Li, T.D. (2009). Preparation and photocatalytic activity of highly ordered mesoporous TiO_2–SBA-15. *Mater. Sci. Eng. C* 29, 1498–1502. DOI: 10.1016/j.msec.2008.12.010.
22. Mazaj, M., Stevens, W.J.J., Zabukovec Logar, N., Ristic, A., Novak Tusar, N., Arcon, I., Daneu, N., Meynen, V., Cool, P., Vansant, E.F. & Kaucic, V. (2009). Synthesis and structural investigations on aluminum-free Ti-Beta/SBA-15 composite. *Micropor. Mesopor. Mater*. 117, 458–465. DOI: 10.1016/j.micromeso.2008.07.025.
23. Henglein, A. (1989). Small-particle research: physicochemical properties of extremely small colloidal metal and semiconductor particles. *Chem. Rev*. 89(8), 1861–1873. DOI: 10.1021/cr00098a010.
24. Capel-Sanchez, M.C., Campos-Martin, J.M., Fierro, J.L.G., de Frutos, M.P. & Padilla Polo, A. (2000). Effective alkene epoxidation with dilute hydrogen peroxide on amorphous silica-supported titanium catalysts. *Chem. Commun*. 855–856. DOI: 10.1039/B000929F.
25. Wróblewska, A. & Makuch, E. (2013). Studies on the deactivation of Ti-MCM-41 catalyst in the process of allyl alcohol epoxidation. *Pol. J. Chem. Technol*. 4(15), 111–115. DOI: 10.2478/pjct-2013-0078.
26. Madhusudan Reddy K., Manorama S.V. & Ramachandra Reddy A. (2003). Bandgap studies on anatase titanium dioxide nanoparticles. *Mater. Chem. Phys*. 78, 239–245. DOI: 10.1016/S0254-0584(02)00343-7.
27. Bahnemann, M.M., Krishna, K.M., Soga, T., Jimbo, T. & Umeno, M. (1999). Optical properties and X-ray photoelectron spectroscopic study of pure and Pb-doped TiO_2 thin films. *J. Phys. Chem. Sol.* 60, 201–210. DOI: 10.1016/S0022-3697(98)00264-9.
28. Rosencwaig, A. (1980). *Photoacoustics and photoacoustic spectroscopy*. New York, John Wiley & Sons, Inc.
29. Nawrocki, J. (1997). The silanol group and its role in liquid chromatography. *J. Chromatogr. A* 779, 29–71. DOI: 10.1016/S0021-9673(97)00479-2.
30. Xie, Y. & Yuan, C. (2003). Visible-light responsive cerium ion modified titania sol and nanocrystallites for X-3B dye photodegradation. *Appl. Catal. B: Environ*. 46, 251–259. DOI: 10.1016/S0926-3373(03)00211-X.
31. Yang, J., Zhang, J., Zhu, L., Chen, S., Zhang, Y., Tang, Y., Zhu, Y. & Li, Y. (2006). Synthesis of nano titania particles embedded in mesoporous SBA-15: Characterization and photocatalytic activity. *J. Hazard. Mater. B* 137, 952–958. DOI: 10.1016/j.jhazmat.2006.03.017.
32. Sun, Z., Bai, C., Zheng, S., Yang. X. & Frost, R.L. (2013). A comparative study of different porous amorphous silica minerals supported TiO_2 catalysts. *Appl. Catal. A: Gen*. 458, 103–110. DOI: 10.1016/j.apcata.2013.03.035.
33. Chen, D. & Ray, A.K. (1999). Photocatalytic kinetics of phenol and its derivatives over UV irradiated TiO_2. *Appl. Catal. B: Environ*. 23, 143–157. DOI: 10.1016/S0926-3373(99)00068-5.
34. Grabowska, E., Reszczyńska, J. & Zaleska, A. (2012). Mechanism of phenol photodegradation in the presence of pure and modified-TiO_2: A review. *Water Res*. 46, 5453–5471. DOI: 10.1016/j.watres.2012.07.048.
35. Turchi, C.S. & Ollis, D.F. (1990). Photocatalytic degradation of organic-water contaminants mechanisms involving hydroxyl radical attack. *J. Catal*. 122, 178–192. DOI: 10.1016/0021-9517(90)90269-P.
36. Zhang, Z., Wang, C.C., Zakaria, R. & Ying, J.Y. (1998). Role of particle size in nanocrystalline TiO_2-photocatalysts. *J. Phys. Chem. B* 102(52), 10871–10878. DOI: 10.1021/jp982948+.
37. Guo, Z., Ma, R. & Li, G. (2006). Degradation of phenol by nanomaterials TiO_2 in wastewater. *Chem. Eng. J*. 119, 55–59. DOI: 10.1016/j.cej.2006.01.017.